J. Fluid Mech. (2008), *vol.* 614, *pp.* 39–65.
doi:10.1017/S0022112008003133 Printed in the United Kingdom

Strongly nonlinear Langmuir circulation and Rayleigh–Bénard convection

G. P. CHINI

Mechanical Engineering Department, University of New Hampshire, Durham, NH 03824, USA

(Received 27 December 2006 and in revised form 25 June 2008)

Most rational asymptotic studies of non-rotating Rayleigh–Bénard convection and its cousins have been restricted to the linear or weakly nonlinear regime. An important exception occurs for large Rayleigh-number thermal convection at effectively infinite Prandtl number, i.e. fast but very viscous convection. In this scenario, the temperature field exhibits a layer-like structure surrounding an isothermal core and, crucially, the momentum equation linearizes. These features have been exploited by several authors to obtain semi-analytical nonlinear solutions. At $O(1)$ Prandtl number, the fluid dynamics in the vortex core is dominated by nonlinear inertial rather than linear viscous effects, substantially altering the vortex structure. Here, it is shown that a combination of matched asymptotic analysis and global conservation constraints can be used to obtain a semi-analytic yet strongly nonlinear description of two related flows: (i) Rayleigh–Bénard convection between constant heat-flux boundaries at unit Prandtl number, and (ii) Langmuir circulation (LC), a wind and wave-driven convective flow commonly observed in natural water bodies. A simple analytical prediction is given for the roll-vortex amplitude, which is shown to be independent of the horizontal wavenumber of the convection pattern. In marked contrast to weakly nonlinear convection cells, the fully nonlinear asymptotic solutions exhibit flow features relevant to turbulent convection including the complete vertical redistribution of the basic-state temperature (or, for LC, downwind velocity) field. Comparisons with well-resolved pseudospectral numerical simulations of the full two-dimensional governing equations confirm the accuracy of the asymptotic results.

1. Introduction

Coherent structures are responsible for much of the turbulent transport of heat, mass and momentum in configurations ranging from Rayleigh–Bénard convection to wall-bounded shear flows. Thus, there is significant interest in predicting the form and dynamics of these flow structures from the governing conservation equations. Waleffe (2001) has coined the phrase 'exact coherent structures' to describe laminar but fully nonlinear exact solutions of the Navier–Stokes equations that exhibit striking similarities with coherent vortical structures observed in wall-bounded turbulent shear flows. Since these solutions are not connected to a primary shear-flow instability, Waleffe and others (Nagata 1990; Faisst & Eckhardt 2003; Kerswell, Tutty & Drazin 2004; Wedin & Kerswell 2004) have devised sophisticated strategies based on homotopy methods to obtain them numerically. Laboratory and numerical experiments strongly suggest that, although unstable, these exact solutions may exert a profound influence on the turbulent dynamics (Faisst & Eckhardt 2004).

In other flows including Rayleigh–Bénard convection and its cousins, remnants of a primary instability mode are evident in the turbulent state. To elucidate the modal structure at high Rayleigh numbers, however, recourse again must be had to numerical continuation methods (see e.g. Mamun & Tuckerman 1995); the majority of analytical studies of convection has been limited to the linear or weakly nonlinear regime. In this regime, the instability modes (often roll vortices) are sufficiently weak that they do not completely restructure the vertical distribution of the horizontally averaged base state, e.g. the mean temperature field. Exceptions occur for rapidly rotating thermal and magnetothermal convection (Bassom & Zhang 1994; Julien & Knobloch 1997; Matthews 1999), circumstances in which the primary instability is to narrow convection cells characterized by a large horizontal wavenumber k when scaled by the inverse depth of the convection zone. Because this length-scale disparity persists into the fully nonlinear regime, where the roll vortices induce an $O(1)$ modification of the mean temperature field, asymptotic methods can be used to obtain a nonlinear eigenvalue problem for the amplitude and vertical structure of the dominant mode. For non-rotating convection with fixed heat-flux boundary conditions, the primary instability is to flat convection cells with small k. In this circumstance, too, an asymptotic theory of nonlinear convection can be developed in which $O(1)$ temperature fluctuations are permitted (Chapman & Proctor 1980). However, the cellular flow field is weak, having $O(k)$ horizontal and $O(k^2)$ vertical velocities, and there is an amplitude/forcing restriction on these long-wavelength asymptotic solutions (see e.g. Cox & Leibovich 1993, 1994, 1997). Furthermore, the $O(1)$ temperature perturbation is depth-independent, implying that the basic-state vertical temperature gradient is not modified at leading order.

These analytical devices are not applicable to classical Rayleigh–Bénard convection, nor to Langmuir circulation – a wind- and surface-wave-driven convective flow commonly observed in natural water bodies (Thorpe 2004). Although Blennerhassett & Bassom (1991), for example, obtain fully nonlinear convection solutions by assuming that k is large, their solutions do not appear to be physically relevant; under strongly supercritical conditions, the dominant cellular mode has an $O(1)$ wavelength (again, when non-dimensionalized by the depth of the convection zone). Analytical progress may still be made, however, by exploiting the weak-diffusion limit. The central idea is not new: in this limit, the vorticity in steady two-dimensional flows with closed streamlines becomes uniform, except in narrow boundary or shear layers, in accord with the Prandtl–Batchelor (PB) theorem (Batchelor 1956; Wood 1957). The value of the constant vorticity can be determined only by accounting for diffusive effects. Generally, this requires the construction of asymptotic solutions in the viscous layers, which must then be matched with the inviscid solution in the vortex core. The resulting PB analysis has been usefully applied to a range of high-Reynolds-number cellular flows governed by the steady two-dimensional Navier–Stokes equations, including cylindrical eddies (Kim 1998), perturbed symmetric eddies (Kim & Childress 2001), and multipolar planar vortices with nonlinear critical layers (Caillol & Grimshaw 2004) and related shear flows in which instabilities give rise to closed (e.g. Kelvin 'cat's-eye') streamline patterns (Maslowe 1986).

Even at finite or zero Reynolds number, when the PB theorem does not hold and the vorticity distribution is non-uniform, steady cellular flows will largely homogenize passive scalar fields in the weak scalar-diffusion limit. Physically, the scalar field is wrapped into a spiral pattern on an advective time scale; the resulting small-scale variability in the scalar field is then smoothed along streamlines over a time period that is short compared to the diffusion time scale. Childress & Gilbert (1995) provide a succinct review of this shear-enhanced diffusive process, which culminates in

cross-streamline diffusion of the scalar on the full diffusive time scale and, ultimately, homogenization of the scalar field within the cell. Since scalar gradients are displaced to the edge of the region of closed streamlines, the process is often referred to as 'flux expulsion'. Rhines & Young (1983) carry out a particularly insightful analysis of the final adjustment stages associated with this phenomenon. Once again, boundary-layer analysis of the periphery of the cellular flow is required to obtain a complete description of the scalar distribution, as is necessary, e.g. to determine the (enhanced) scalar flux through the cell. These ideas have been exploited by numerous investigators in a variety of contexts. Lingevitch & Bernoff (1994) analysed the advection of a passive scalar by an isolated vortex couple using a WKB averaging approach to capture the initial homogenization along streamlines and the slower diffusion across them; boundary-layer analysis was employed to determine the scalar flux from the couple into the surrounding flow. In earlier studies of dynamos, Childress (1979), Soward (1987) and Perkins & Zweibel (1987) carried out similar boundary-layer analyses, while Shraiman (1987) used related techniques to quantify the order-of-magnitude enhancement in the diffusive transport of a passive impurity by a periodic array of steady two-dimensional convection cells. The present investigation employs a similar matched asymptotic approach, but extends these (and other – see below) earlier analyses by determining rather than prescribing the cellular flow and by treating an active rather than a passive scalar field.

In the case of Rayleigh–Bénard convection at finite or low Prandtl number and large Rayleigh number, many authors have suggested scalings for the various flow sub-domains (see e.g. Moore & Weiss 1973), but, evidently, none has succeeded in constructing a rational asymptotic solution. Busse & Clever (1981), for example, developed a model of two-dimensional convection valid in the limit of small Prandtl number, but they assumed rather than solved for the rotational core motion. Several authors (Roberts 1979; Olson & Corcos 1980; Jimenez & Zufiria 1987) have made more analytical progress in the case of infinite-Prandtl-number Rayleigh–Bénard convection, in which, crucially, the momentum equation linearizes. Although the cellular flow is viscous and, hence, the vorticity in the core non-uniform, the temperature field in the large-Rayleigh-number limit is composed of an isothermal core surrounded by thin thermal boundary layers and plumes. Jimenez & Zufiria (1987), in particular, carried out a careful boundary-layer analysis of this problem, resolving singularities that appear near the corners of the cell. They obtained a semi-analytic solution for the flow fields and computed an asymptotic relationship between the scaled Nusselt number and the wavelength of the convection pattern. In the Langmuir circulation context, Li & Garrett (1993) proposed asymptotic scalings in the weak-diffusion–strong-forcing limit based on their fully nonlinear numerical simulations, but they did not attempt to construct an asymptotic solution.

Here, we study the weak-diffusion limit of the Craik–Leibovich (CL) equations (Craik & Leibovich 1976; Craik 1977; Leibovich 1977), the broadly accepted theoretical model of Langmuir circulation. The CL equations are a surface-wave filtered version of the Navier–Stokes equations in which the rectified effects of the waves appear in a vortex force term. This force is given by the cross-product of the Stokes drift, i.e. the Lagrangian mass drift associated with the filtered surface waves, and the averaged Eulerian vorticity vector. In the small 'laminar Langmuir number' (La) limit of interest, vorticity production by the CL vortex force dominates small-scale diffusion. In fact, McWilliams, Sullivan & Moeng (1997) have argued that their 'turbulent Langmuir number' is a more appropriate system parameter, since oceanographic estimates suggest that La is typically much less than unity. By

exploiting the limit $La \to 0$, we are able to elucidate the asymptotic structure of steady, strongly forced Langmuir circulation (LC) and to obtain a strikingly simple prediction for the value $\bar{\Omega}$ of the (constant) vorticity in the inviscid vortex core, which is shown to be independent of the LC wavenumber k.

When the flow is downwind-invariant (i.e. two-dimensional) and the vertical Stokes-drift gradient is constant, as assumed here, there is a strict mathematical analogy between Langmuir circulation and two-dimensional Rayleigh–Bénard convection (RBC) at unit Prandtl number. The LC downwind velocity component corresponds to the total temperature field in RBC; the physical boundary conditions assumed here for LC correspond to fixed heat-flux thermal convection between stress-free horizontal boundaries. Thus, our results are equally applicable to RBC under these conditions. We borrow certain ideas from the work of Jimenez & Zufiria (1987), but emphasize that the effective Prandtl number in our problem is unity; hence, we treat a completely nonlinear system of equations. At $O(1)$ rather than infinite Prandtl number, the fluid dynamics in the vortex core is dominated by nonlinear inertial rather than linear viscous effects, substantially altering the vortex structure.

At sufficiently small La, the steady solutions we investigate are undoubtedly unstable; indeed, Langmuir circulation is properly viewed as part of the near-surface ocean turbulence. In part, our purpose is similar in spirit to that of Waleffe (2001), except that we seek 'asymptotic' rather than exact coherent structures. Kawahara & Kida (2001), like Waleffe, have also numerically computed unstable (time-periodic rather than steady) solutions in a wall-bounded shear flow. These authors demonstrate that the mean velocity profile and root-mean-square velocity fluctuations in low-Reynolds-number Couette turbulence can be predicted well with their unstable solutions. Beyond a similar potential merit of our analysis, however, our investigation addresses a fundamental question that we deem to be of intrinsic theoretical interest. Accordingly, our primary aim is to construct a semi-analytic solution describing strongly nonlinear convection in the weak diffusion limit.

The organization of the paper is as follows. In § 2, we state the equations and boundary conditions governing steady two-dimensional LC and the equivalent system for RBC. High-resolution pseudospectral numerical solutions are briefly described in § 3; the structure of these solutions motivates the scalar homogenization analysis given in § 4 and the matched asymptotic analysis carried out in § 5. Using the asymptotic scalings developed in the preceding sections, a combination of global momentum and energy constraints is used in § 6 to determine the constant core vorticity ($\bar{\Omega}$) – this constant is one of the central unknowns in the analysis, as it governs the strength of the cellular flow. With $\bar{\Omega}$ determined, a 'Childress-like' cell problem (Childress 1979) for the LC downwind velocity component (or, for RBC, the temperature) is formulated and solved analytically in § 7. In § 8, an efficient numerical scheme for generating the steady strongly nonlinear convective states is developed by exploiting semi-analytical knowledge of the solution structure; these semi-analytical solutions are shown to agree closely with full numerical solutions. We conclude in § 9 by summarizing our results and outlining several related open problems.

2. Problem formulation

2.1. *Langmuir circulation*

We look for steady two-dimensional nonlinear solutions of the CL equations. In streamfunction–vorticity form, these equations can be expressed as

$$\frac{\partial \psi}{\partial z}\frac{\partial v_x}{\partial y} - \frac{\partial \psi}{\partial y}\frac{\partial v_x}{\partial z} = La\left[\frac{\partial^2 v_x}{\partial y^2} + \frac{\partial^2 v_x}{\partial z^2}\right], \tag{2.1}$$

$$\frac{\partial \psi}{\partial z}\frac{\partial \Omega}{\partial y} - \frac{\partial \psi}{\partial y}\frac{\partial \Omega}{\partial z} = -\frac{\mathrm{d}U_s}{\mathrm{d}z}\frac{\partial v_x}{\partial y} + La\left[\frac{\partial^2 \Omega}{\partial y^2} + \frac{\partial^2 \Omega}{\partial z^2}\right], \tag{2.2}$$

$$\frac{\partial^2 \psi}{\partial y^2} + \frac{\partial^2 \psi}{\partial z^2} = -\Omega, \tag{2.3}$$

where x is the downwind direction, y is the cross-wind coordinate and z is directed vertically upward with $z = 0$ coincident with the mean position of the air–sea interface. All flow-fields are assumed to be steady and x-invariant: $v_x(y, z)$ is the total downwind current; $v(y, z) \equiv \partial\psi(y, z)/\partial z$ and $w(y, z) \equiv -\partial\psi(y, z)/\partial y$ are the horizontal and vertical cross-wind velocity components, respectively; and $\Omega \equiv \partial w/\partial y - \partial v/\partial z$ is the x-component of the vorticity. The total downwind velocity field is comprised of a basic-state shear flow $U_b(z) \equiv z + 1$, which carries the applied wind stress, and a finite-amplitude perturbation $u(y, z)$ to that base flow, i.e. $v_x(y, z) \equiv U_b(z) + u(y, z)$. The non-dimensional Stokes-drift velocity gradient $\mathrm{d}U_s/\mathrm{d}z \equiv 1$. Although an exponentially decaying Stokes drift profile is more appropriate for LC in the open ocean, we employ a linear profile because (i) the required matched asymptotic analysis is simpler in this case, for reasons discussed in the next section, and (ii) the two-dimensional CL equations are then formally identical to the two-dimensional Oberbeck–Boussinesq equations governing RBC, as discussed in § 2.2.

In (2.1)–(2.3), y and z have been scaled by the depth H of the convective zone; v_x, u and U_b each have been scaled by $u_* R_*$, where u_* is the water friction velocity (with u_*^2 equal to the magnitude of the wind stress divided by the water density), $R_* \equiv u_* H/\nu_e$ is a friction Reynolds number and ν_e is an assumed constant eddy viscosity (Leibovich 1977, 1980); and v and w have been scaled by $[u_* R_* u_{s_0}]^{1/2}$, where u_{s_0} is the (dimensional) Stokes-drift velocity scale, here defined to equal the product of H and the dimensional surface value of the Stokes-drift gradient. One non-dimensional parameter appears in (2.1)–(2.3): the laminar Langmuir number,

$$La \equiv \frac{\nu_e}{[u_* R_* u_{s_0}]^{1/2} H} = \left[\frac{1}{R_*^3 S}\right]^{1/2}, \tag{2.4}$$

where $S \equiv u_{s_0}/u_*$ is the non-dimensional Stokes-drift velocity scale.

The eddy viscosity appearing in La arises from the wave-filtering procedure used in the derivation of the CL equations. Estimates nevertheless suggest that $La \ll 1$ in wind-forced seas (Li & Garrett 1993; McWilliams *et al.* 1997), with a typical value being in the range $O(10^{-3})$–$O(10^{-4})$. Here, we formally exploit the asymptotic limit $La \to 0$ to obtain a semi-analytic characterization of strongly nonlinear Langmuir circulation; this approach should provide an important complement to the more common weakly nonlinear descriptions of convection.

Boundary conditions are imposed at the mean position of the air–sea interface $z = 0$ and at the base of the convective region $z = -1$. Following Leibovich (1983), we assume the perturbation stresses vanish at these planes. In addition, the numerical solutions described in § 3 impose horizontal periodicity; when these solutions reach a steady state, they exhibit reflection symmetry. Thus, we impose the following boundary and symmetry conditions in our analysis:

$$z = 0, -1 : \frac{\partial u}{\partial z} = 0 \left(\text{i.e. } \frac{\partial v_x}{\partial z} = 1\right), \ \psi = 0, \ \Omega = 0, \tag{2.5}$$

$$y = 0, \pi/k : \frac{\partial u}{\partial y} = 0 \left(\text{i.e. } \frac{\partial v_x}{\partial y} = 0\right), \ \psi = 0, \ \Omega = 0, \tag{2.6}$$

where π/k is the horizontal width of a single steady Langmuir cell. Note that the wavenumber k is a specified input to this analysis; above the primary instability threshold, cellular modes with wavenumbers within a continuous band are possible. Our analysis does not predict a preferred wavelength, although incorporation of large-scale modulation of these nonlinear modes may provide a wavenumber selection mechanism (see e.g. Newell, Passot & Souli 1990). Moreover, the analysis of Cox & Leibovich (1993) indicates that the critical wavenumber k_c of the primary (linear) instability mode is zero for the given zero perturbation-stress boundary conditions, a prediction that is not remedied by weak nonlinearity. Nevertheless, for La^{-1} sufficiently greater than La_c^{-1}, the fastest-growing mode has an $O(1)$ wavenumber. Indeed, under strongly supercritical forcing conditions characteristic of typical wind-forced seas, our simulations in a periodic y-domain invariably reach a saturated state in which the Langmuir circulation has a finite, not infinite, wavelength: in sufficiently wide computational domains, more than two cells are observed in the final steady state. Similar issues arise in other convection problems, e.g. binary fluid convection, where steady convection sets in at $k_c = 0$ but numerically computed nonlinear states have finite k even relatively close to onset.

2.2. *Rayleigh–Bénard convection*

As mentioned above, when the Stokes-drift gradient is constant, there is a strict mathematical analogy between the downwind invariant CL equations and the two-dimensional Oberbeck–Boussinesq equations governing RBC at unit Prandtl number. We exploit this analogy by setting $\mathrm{d}U_s/\mathrm{d}z = 1$ in (2.2), for then (2.1)–(2.3) can be recast as

$$\frac{\partial\psi}{\partial z}\frac{\partial T}{\partial y} - \frac{\partial\psi}{\partial y}\frac{\partial T}{\partial z} = \hat{R}^{-1/2}\left[\frac{\partial^2 T}{\partial y^2} + \frac{\partial^2 T}{\partial z^2}\right], \tag{2.7}$$

$$\frac{\partial\psi}{\partial z}\frac{\partial \Omega}{\partial y} - \frac{\partial\psi}{\partial y}\frac{\partial \Omega}{\partial z} = \frac{\partial T}{\partial y} + \hat{R}^{-1/2}\left[\frac{\partial^2 \Omega}{\partial y^2} + \frac{\partial^2 \Omega}{\partial z^2}\right], \tag{2.8}$$

$$\frac{\partial^2\psi}{\partial y^2} + \frac{\partial^2\psi}{\partial z^2} = -\Omega, \tag{2.9}$$

upon identifying the LC downwind velocity component $v_x(y, z)$ with the negative of the temperature anomaly, $T(y, z)$, in RBC. (The definitions of $\Omega(y, z)$ and $\psi(y, z)$ are unchanged.) In the RBC context, (2.5) corresponds to specified heat-flux conditions along planar stress-free boundaries. For constant heat-flux RBC, the 'effective' Rayleigh number $\hat{R} \equiv \alpha g \beta H^4/(\nu\kappa)$, where α, g, ν, κ and β are the thermal expansion coefficient, the acceleration due to gravity, the molecular viscosity, the molecular thermal diffusivity and the temperature gradient imposed at the upper (or lower) boundary, respectively. To complete the analogy, we require $\hat{R} = La^{-2}$ in (2.7) and (2.8). Thus, a Langmuir number of 10^{-4}, the smallest La for which we carried out full numerical simulations (see § 3), corresponds to $\hat{R} = 10^8$ – again, at unit Prandtl number. (Otero *et al.* (2002) demonstrate that the conventional Rayleigh number Ra, defined in terms of the temperature drop across the layer, is related to the effective Rayleigh number via the relation $Ra = \hat{R}|\Delta T|$, where ΔT is the horizontal-mean temperature difference between the upper and lower boundaries. Using a scaling for the *a priori* unknown ΔT implied by the subsequent analysis, it can be shown that $Ra = O(La^{-3/2})$ as $La \to 0$ and, hence, that $\hat{R} = 10^8$ corresponds to $Ra = O(10^6)$.) Given this re-interpretation of variables, the results of the present investigation are equally applicable to LC and to RBC under the stated conditions.

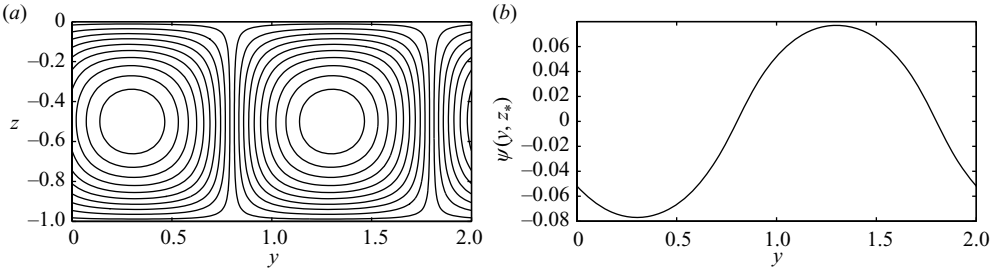

FIGURE 1. (*a*) Contour plot of cross-wind streamfunction ψ in steady state for $La = 0.0012$. Positive contour values (right cell) increase monotonically from 0.00368 at the cell perimeter to 0.0700 in the cell interior in increments of 0.00737. (*b*) Plot of ψ as a function of the cross-wind coordinate y at the cell mid-depth $z_* = -1/2$ showing that, in contrast to the downwind vorticity (see figure 2), the streamfunction is smooth and, in fact, nearly harmonic.

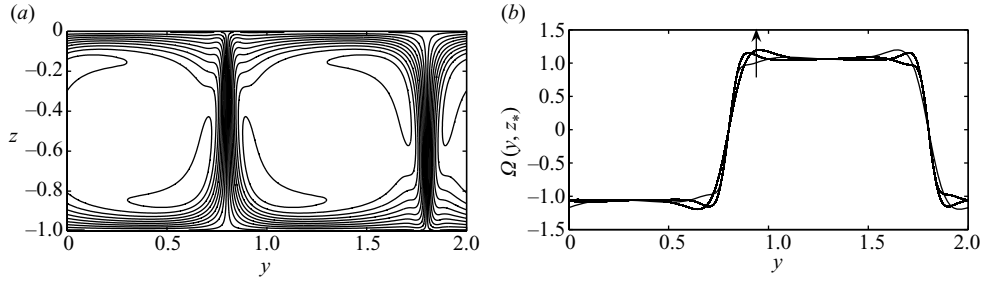

FIGURE 2. (*a*) Contour plot of downwind vorticity Ω in steady state for $La = 0.0012$. Positive contour values (right cell) increase monotonically from 0.0595 at the cell perimeter to 1.13 along the interior lobes in increments of 0.119. (*b*) Plots of Ω as a function of the cross-wind coordinate y for depths $z_* = -1/4$, $z_* = -1/2$ and $z_* = -3/4$. The arrow labelling these curves indicates the direction of decreasing z_* (i.e. increasing depth). Note that Ω is nearly uniform away from the perimeter of each cell.

3. Time-dependent numerical simulations

We implemented a pseudospectral Fourier–Chebyshev code to solve the time-dependent versions of (2.1)–(2.3), subject to a horizontal periodicity constraint and boundary conditions (2.5). The linear terms are advanced using the semi-implicit Crank–Nicolson scheme, while the nonlinear and instability terms are advanced using the fully explicit second-order Adams–Bashforth method. The resulting system of linear algebraic equations is solved via matrix diagonalization techniques. The code has been fully tested and yields results that agree closely with other independently developed Langmuir circulation solvers. For the given boundary conditions, sustained convection first occurs at a critical Langmuir number $La_c = 1/\sqrt{120} \approx 0.0913$ (Cox & Leibovich 1993). When La^{-1} is less than $O(10^4)$ but greater than La_c^{-1}, a range of k values can be specified for which white noise initial conditions evolve into steady cellular flows that are unique to within an arbitrary cross-wind phase shift. Figures 1–3 show a typical solution in steady state, computed for $La = 0.0012$ (i.e. almost two orders of magnitude less than La_c), $k = \pi$ and $\mathrm{d}U_s/\mathrm{d}z = 1$ using 64 Fourier and 75 Chebyshev modes.

Several features of this small-La solution are noteworthy. First, these solutions clearly are strongly nonlinear, as evidenced by the sharp jumps in the downwind vorticity (see figure 2*b*) and by the complete vertical and horizontal redistribution

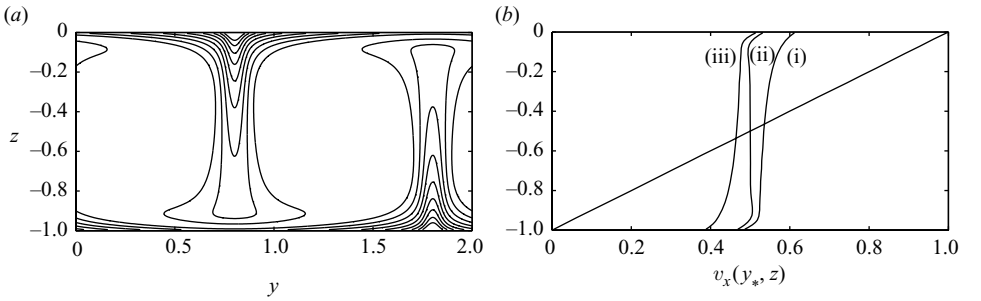

FIGURE 3. (*a*) Contour plot of total downwind velocity v_x (or, for RBC, negative of the temperature anomaly T) in steady state for $La = 0.0012$. Contours in the downwelling zone centred at $y \approx 0.8$ decrease monotonically from 0.59 near $z = 0$ to 0.51 near $z = -1$ in increments of 0.01; the corresponding contours in the upwelling zone centred at $y \approx 1.8$ increase monotonically from 0.41 near $z = -1$ to 0.49 near $z = 0$ in increments of 0.01. (*b*) Plots of v_x as a function of depth z for three different cross-wind sections: (i) $y_* = 0.80$ (downwelling zone); (ii) $y_* = 1.3$ (middle of the right cell); and (iii) $y_* = 1.8$ (upwelling zone). For comparison, the diagonal line shows the basic-state wind-driven shear flow (or, for RBC, the negative of the linear conduction profile). Note that the vortices completely redistribute the downwind momentum (temperature) in the basic state.

of the downwind momentum (or, for RBC, temperature) contained in the basic state (see figure 3*b*). The near constancy of the mean (e.g. time-averaged) core temperature in large-Ra RBC and the concomitant generation of thermal boundary layers has long been observed in experiments (e.g. Deardorff & Willis 1967); predicted by the early modelling studies of Gough, Spiegel & Toomre (1975) based on their 'single-mode' convection equations (also see Toomre, Gough & Spiegel 1977); and identified in the full numerical simulations of the two-dimensional Oberbeck–Boussinesq equations by Moore & Weiss (1973). In contrast, weakly nonlinear convection cells exhibit sinusoidal spatial variability and do not modify the basic state at leading order. Nevertheless, figure 1 shows that the streamfunction remains smooth and varies roughly harmonically in the cross-wind direction; the smooth character of the streamfunction is exploited in both the asymptotic analysis and the construction of hybrid analytical–numerical solutions described in subsequent sections. Next, there is clear evidence of an asymptotic structure characterized by near-surface and bottom boundary layers, narrow downwelling and upwelling zones, corner regions and a nearly inviscid rotational core. Finally, in addition to being invariant under arbitrary translations in y, the equations and boundary conditions governing the computational problem are invariant under a 180° rotation: $(y, z) \rightarrow (-y, -z-1)$, $(v_x, \Omega, \psi) \rightarrow (1 - v_x, \Omega, \psi)$. Specifically, if a steady nonlinear spatially periodic convective state $[v_x(y, z), \psi(y, z), \Omega(y, z)]$ is obtained with the mid-plane of an up- or downwelling zone located along the z-axis, then $[1 - v_x(\pi/k - y, -z-1), \psi(\pi/k - y, -z-1), \Omega(\pi/k - y, -z-1)]$ is also a solution of (2.1)–(2.3) and (2.5)–(2.6), as is visually evident in the contour plots in figures 1–3. This discrete rotational symmetry is broken whenever the Stokes-drift gradient is not constant, as for Langmuir circulation in the open ocean; downwelling zones are then somewhat narrower and more intense than upwelling regions, in accord with ocean observations. Here, we focus on the constant Stokes-drift-gradient scenario, i.e. $\mathrm{d}U_s/\mathrm{d}z = 1$ in (2.2); thus, we search for solutions possessing this symmetry. This case should be more tractable analytically because the numerical solutions indicate that $\Omega(y, z)$ is nearly uniform in the inviscid vortex core (see figure 2): when $\mathrm{d}U_s/\mathrm{d}z$ is

constant, steady two-dimensional Langmuir cells – which satisfy the CL rather than Navier–Stokes equations – obey a Prandtl–Batchelor theorem in the small-La limit (see § 4), greatly simplifying the required asymptotic matching. The simulations of Li & Garrett (1993) suggest that this may not be the case when the Stokes-drift gradient varies (but see § 4).

4. Scalar homogenization

The numerical experiments described in § 3 suggest that, for $La \ll 1$, a steady state exists with viscous layers surrounding an inviscid core in which both $v_x(y, z)$ and $\Omega(y, z)$ are homogenized. As shown below, these observations follow from a small-La analysis of certain integral constraints derivable from (2.1)–(2.3). The homogenization results are then exploited in the subsequent analysis.

First, integrating (2.1) from $y = 0$ to $y = \pi/k$ and from $z = -1$ to $z = z_*$ (an arbitrary depth within the domain) and using the divergence theorem yields

$$\oint_C v_n v_x \, \mathrm{d}l = La \oint_C \frac{\partial v_x}{\partial n} \, \mathrm{d}l, \tag{4.1}$$

where C is the curve bounding the spatial domain of integration, $\mathrm{d}l$ is an element of arclength along C, and v_n is the velocity component normal to C. Evaluating these integrals and noting that the zero perturbation-flux boundary condition in (2.5) can be expressed as $\partial v_x/\partial z = 1$ at $z = -1$ (and $z = 0$) gives the following exact formula:

$$La \frac{\pi}{k} = \int_0^{\pi/k} \left(La \frac{\partial v_x}{\partial z} - w v_x \right) \Big|_{z=z_*} \mathrm{d}y. \tag{4.2}$$

This equation indicates that for a steady flow to be realized, the vertical flux of downwind momentum, integrated across the cell, must be constant (i.e. independent of z), given the symmetry constraints at $y = 0$ and $y = \pi/k$.

Next, we demonstrate that v_x is homogenized in the vortex core as $La \to 0$. Often referred to as 'flux expulsion' or 'scalar homogenization', this process is known to govern the long-time distribution of passive scalars in a two-dimensional cellular flow field in the weak-diffusion limit (see e.g. Rhines & Young 1983). Following standard arguments, we show the same result holds for the active scalar field $v_x(y, z)$. Integrating (2.1) over an area of the cellular flow and using the divergence theorem again yields (4.1). Upon selecting the closed curve C to be a streamline (so $v_n = 0$ on C), the exact result

$$La \oint_C \frac{\partial v_x}{\partial n} \, \mathrm{d}l = 0 \tag{4.3}$$

is obtained. This result holds for all La and, thus, is valid in the limit as $La \to 0$. Viscous forces are negligible in that limit, except in horizontal boundary layers and vertical jets and plumes. In the inviscid core, (2.1) simplifies to

$$\frac{\partial \psi}{\partial z} \frac{\partial v_x}{\partial y} - \frac{\partial \psi}{\partial y} \frac{\partial v_x}{\partial z} = 0, \tag{4.4}$$

which (abusing notation) has the solution $v_x = v_x(\psi)$. Thus, in the small-La limit, and for C in the inviscid core, (4.1) becomes

$$0 = \oint_C v_x'(\psi) \frac{\partial \psi}{\partial n} \, \mathrm{d}l = v_x'(\psi) \oint_C \frac{\partial \psi}{\partial n} \, \mathrm{d}l, \tag{4.5}$$

where the prime denotes ordinary differentiation, implying $v_x'(\psi)\Gamma_C = 0$. Since the circulation Γ_C around C is non-zero,

$$v_x = \bar{U}, \tag{4.6}$$

a constant, in the core. We note that (4.6) satisfies (2.1) to all algebraic orders in La. (In § 5, it is shown that $v_x(y, z)$ satisfies a diffusion equation in suitably rescaled and transformed coordinates in the viscous layers around the cell perimeter; thus, no corrections algebraic in La are forced in the interior.) In fact, given the problem specification, any spatially uniform downwind velocity component can be added to a solution of (2.1)–(2.3) with boundary conditions (2.5)–(2.6) and the result is also a solution. Thus, without loss of generality, we are at liberty to set $\bar{U} \equiv 1/2$.

Finally, using the homogenization of v_x, we can demonstrate that a Prandtl–Batchelor theorem holds for the two-dimensional Craik–Leibovich (rather than the two-dimensional Navier–Stokes) equations. In vector form, the steady two-dimensional CL equations can be written as

$$\boldsymbol{v}\cdot\nabla\boldsymbol{v} = -\nabla\pi + \boldsymbol{U}_s\times\boldsymbol{\omega} + La\nabla^2\boldsymbol{v},$$

or, equivalently, as

$$\boldsymbol{\omega}\times(\boldsymbol{v}+\boldsymbol{U}_s) = -\nabla\left(\pi + \frac{|\boldsymbol{v}|^2}{2}\right) - La(\nabla\times\boldsymbol{\omega}), \tag{4.7}$$

where π is a filtered (surface-wave modified) pressure, and

$$\boldsymbol{v} = v_x\hat{\imath} + v\hat{\jmath} + w\hat{k}, \tag{4.8}$$

$$\boldsymbol{\omega} = \Omega\hat{\imath} + \omega_y\hat{\jmath} + \omega_z\hat{k} = \left(\frac{\partial w}{\partial y} - \frac{\partial v}{\partial z}\right)\hat{\imath} + \left(\frac{\partial v_x}{\partial z}\right)\hat{\jmath} + \left(-\frac{\partial v_x}{\partial y}\right)\hat{k}, \tag{4.9}$$

and $\nabla\cdot\boldsymbol{v} = 0$. Taking the dot product of (4.7) with an infinitesimal displacement vector $\mathrm{d}\boldsymbol{l}$ tangent to a streamline in the (y,z)-plane, and then integrating around a closed streamline C, yields the following exact result:

$$\oint_C U_s\left(\frac{\partial v_x}{\partial y}\hat{\jmath} + \frac{\partial v_x}{\partial z}\hat{k}\right)\cdot\mathrm{d}\boldsymbol{l} = La\oint_C\left(\frac{\partial\Omega}{\partial z}\hat{\jmath} - \frac{\partial\Omega}{\partial y}\hat{k}\right)\cdot\mathrm{d}\boldsymbol{l}. \tag{4.10}$$

Equation (4.10) is a statement of energy balance: the work done by the CL vortex (or buoyancy) force as the flow traverses a closed loop C (the left-hand side) is balanced by the frictional dissipation of the kinetic energy of the motion along that path (the right-hand side). Again, this statement holds for any La and, in particular, is valid as $La\to 0$. In that limit, v_x in the core is uniform to all algebraic orders; hence, along a circuit C coincident with any closed streamline within the core, the left-hand side of (4.10) is exponentially small in La, implying

$$\oint_C\left(\frac{\partial\Omega}{\partial z}\hat{\jmath} - \frac{\partial\Omega}{\partial y}\hat{k}\right)\cdot\mathrm{d}\boldsymbol{l} = 0. \tag{4.11}$$

The vorticity equation (2.2) in the inviscid core becomes

$$\frac{\partial\psi}{\partial z}\frac{\partial\Omega}{\partial y} - \frac{\partial\psi}{\partial y}\frac{\partial\Omega}{\partial z} = 0, \tag{4.12}$$

since, crucially, v_x is constant there. Thus, $\Omega = \Omega(\psi)$, implying

$$\Omega'(\psi)\oint_C(v\hat{\jmath} + w\hat{k})\cdot\mathrm{d}\boldsymbol{l} = \Omega'(\psi)\Gamma_C = 0. \tag{4.13}$$

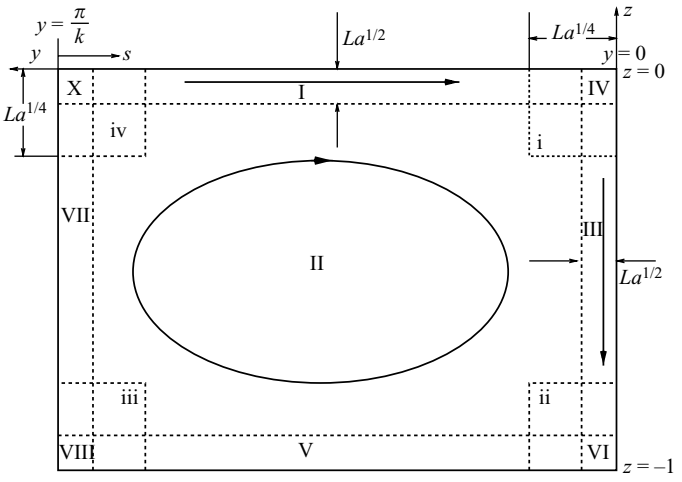

FIGURE 4. Hypothesized multi-region asymptotic structure of a steady Langmuir cell as $La \to 0$. Note that the coordinate s introduced in § 5 increases in the negative y-direction for positive $\bar{\Omega}$, with the origin $s = 0$ situated at the top of the upwelling zone (in the upper left-hand corner of the cell).

Noting that the circulation Γ_C around the streamline C is non-zero, we deduce that

$$\Omega = \bar{\Omega}, \tag{4.14}$$

a constant, in the vortex core; that is, this flow satisfies a Prandtl–Batchelor (PB) theorem. Physically, as $La \to 0$, the CL vortex (or buoyancy) torque vanishes in the vortex core, allowing weak viscous effects to homogenize the vorticity.

It is shown in § 5 that $\Omega(y, z)$ also satisfies diffusion equations in the viscous layers at the edges of the cell; like $v_x(y, z)$, $\Omega(y, z)$ therefore is asymptotic to a constant in the vortex core to all algebraic orders in La. Unlike $\bar{U}$, however, the value of $\bar{\Omega}$ is not arbitrary and must be determined in the course of the analysis. We observe that the exact form of the Stokes-drift velocity does not explicitly enter the above derivation; thus, the PB theorem is expected to hold for flows with more realistic, exponentially decaying Stokes drift profiles. The key assumption, perhaps implicitly influenced by the form of $U_s(z)$, is that there exists a family of closed streamlines that is bounded away from regions of viscous dissipation. If, on the contrary, all streamlines pass through a viscous layer, then the above arguments fail, and the PB theorem will not necessarily hold.

5. Asymptotic analysis

The numerical solutions presented in § 3 and the homogenization results derived in § 4 motivate the hypothesized small-La asymptotic structure shown in figure 4. In the subsections that follow, we describe the distinguished limits that characterize the various subregions of the flow, obtain and analytically solve simplified equations in these regions, and demonstrate that the solutions can be asymptotically matched from one subdomain to the next.

5.1. *Region II. Inviscid vortex core*

Over the bulk of the domain, the flow behaves inviscidly. Keeping y, z fixed, letting $La \to 0$ and recalling (4.6) and (4.14), we find that

$$v_x(y,z) \sim \bar{U} + E.S.T., \tag{5.1}$$

$$\psi(y,z) \sim \psi_{II}(y,z) + La^{1/2}\psi_{II}^{(1)}(y,z), \tag{5.2}$$

$$\Omega(y,z) \sim \bar{\Omega} + E.S.T., \tag{5.3}$$

where $E.S.T.$ refers to terms exponentially small in La, satisfy the governing equations although not all of the boundary conditions. As a consequence of (5.3), $\psi_{II}(y,z)$ satisfies

$$\frac{\partial^2\psi_{II}}{\partial y^2} + \frac{\partial^2\psi_{II}}{\partial z^2} = -\bar{\Omega}, \tag{5.4}$$

subject to the boundary conditions that $\psi_{II}(y,z) = 0$ along $z = 0, -1$ and $y = 0, \pi/k$. The solution can be expressed as an infinite series:

$$\psi_{II}(y,z) = \sum_{n=1}^{\infty} \psi_n(z)\,\sin(nky), \tag{5.5}$$

where n is an odd integer and

$$\psi_n(z) = \frac{4\bar{\Omega}}{\pi k^2 n^3}\left[1 - \frac{\cosh\left(nk\left(z+\frac{1}{2}\right)\right)}{\cosh(nk/2)}\right]. \tag{5.6}$$

Since only odd n appear in the infinite sum, the magnitude of the second term in the series is only about $1/27$ that of the $n = 1$ term; i.e. $\psi_{II}(y,z)$ is nearly a pure sinusoid in y, as we have verified via comparisons with the numerical solutions (see figure 1).

For matching with both the near-surface boundary layer and the downwelling jet, the behaviour of $\psi_{II}(y,z)$ as y and z separately approach zero is required. Assuming

$$\psi(y,z) \sim \psi_{II}(y,0) + z\,\frac{\partial\psi_{II}}{\partial z}(y,0) \quad \text{as } z \to 0^-,$$

$$\psi(y,z) \sim \psi_{II}(0,z) + y\,\frac{\partial\psi_{II}}{\partial y}(0,z) \quad \text{as } y \to 0^+,$$

i.e. that

$$\psi(y,z) \sim v_{II}(y,0)\,z \quad \text{as } z \to 0^-, \tag{5.7}$$

$$\psi(y,z) \sim -w_{II}(0,z)\,y \quad \text{as } y \to 0^+, \tag{5.8}$$

leading-order matching of $\psi(y,z)$ between the viscous layers and the interior is readily accomplished. Using (5.5) and (5.6), we obtain:

$$v_{II}(y,0) = \sum_{n=1}^{\infty}\left(-\frac{4\bar{\Omega}}{\pi k n^2}\right)\tanh\left(\frac{nk}{2}\right)\sin(nky), \tag{5.9}$$

and

$$w_{II}(0,z) = \sum_{n=1}^{\infty}\left(-\frac{4\bar{\Omega}}{\pi k n^2}\right)\left[1 - \frac{\cosh\left(nk\left(z+\frac{1}{2}\right)\right)}{\cosh(nk/2)}\right], \tag{5.10}$$

where the sums are again taken only over odd n.

Finally, we emphasize that the total downwind velocity $v_x(y, z) = U_b(z)+u(y, z) \sim \bar{U}$ is constant in the bulk interior of the convecting layer (see figure 3). Unlike weakly nonlinear roll vortices, fully nonlinear Langmuir cells completely restructure the wind-driven basic-state shear flow.

5.2. *Region I. Near-surface boundary layer*

To satisfy the tangential-stress and flux conditions, boundary layers must exist near the free surface and the base of the layer. Owing to the rotational symmetry of the problem, we need only consider the $z = 0$ boundary layer, where the vertical length scale must be $O(La^{1/2})$ for vertical diffusion of momentum to balance advection. Using the divergence-free condition, the streamfunction also is found to be $O(La^{1/2})$, confirming that relatively little fluid passes through the thin layer. Although the numerical simulations indicate that the near-surface downwind velocity perturbation $u(y, z)$ is $O(1)$ (again, see figure 3), the deviation of $v_x(y, z)$ from the core value $\bar{U}$ is $O(La^{1/2})$. This scaling is most easily deduced from the constant flux condition in (2.5). One important implication is that the vertical vorticity is asymptotically small within the near-surface and bottom boundary layers. Finally, the numerics reveal that the downwind vorticity achieves $O(1)$ values within the surface boundary layer. (For sufficiently small La, the numerical simulations indicate that the downwind vorticity reaches a maximum at the edge of the boundary layer, then decreases and asymptotes to a constant value within the inviscid core; see figure 2.) Thus, we propose

$$v_x(y, z) \sim \bar{U} + La^{1/2}u_I(y, Z), \tag{5.11}$$

$$\psi(y, z) \sim La^{1/2}\psi_I(y, Z), \tag{5.12}$$

$$\Omega(y, z) \sim \Omega_I(y, Z), \tag{5.13}$$

where $Z \equiv z/La^{1/2}$. Taking the inner limit of (2.1)–(2.3), with y, Z fixed as $La \to 0$, we obtain the leading-order equations

$$\frac{\partial^2\psi_I}{\partial Z^2} = 0 \;\Rightarrow\; \psi_I(y, Z) = V(y)Z, \tag{5.14}$$

$$\frac{\partial^2 u_I}{\partial Z^2} = V(y)\frac{\partial u_I}{\partial y} - V'(y)Z\frac{\partial u_I}{\partial Z}, \tag{5.15}$$

$$\frac{\partial^2\Omega_I}{\partial Z^2} = V(y)\frac{\partial\Omega_I}{\partial y} - V'(y)Z\frac{\partial\Omega_I}{\partial Z}, \tag{5.16}$$

where a prime denotes ordinary differentiation. Comparing (5.12) and (5.14) with (5.7), we observe that $\psi(y, z)$ in the boundary layer can be matched with the interior solution by setting $V(y) = v_{II}(y, 0)$ given in (5.9). Moreover, with $\psi_I(y, Z)$ known (to within the constant factor $\bar{\Omega}$), the boundary-layer equations (5.15) and (5.16) for $u_I(y, Z)$ and $\Omega_I(y, Z)$ linearize – a crucial simplification. Because the vertical vorticity is weak, these equations decouple. Equation (5.15) must be solved subject to the boundary conditions

$$\frac{\partial u_I}{\partial Z}(y, 0) = 1, \tag{5.17}$$

$$u_I(y, Z) \to 0 \quad \text{as } Z \to -\infty, \tag{5.18}$$

while the boundary conditions for (5.16) are

$$\Omega_I(y, 0) = 0, \tag{5.19}$$

$$\Omega_I(y, Z) \to \bar{\Omega} \quad \text{as } Z \to -\infty. \tag{5.20}$$

The advection–diffusion equations (5.15), (5.16) with conditions (5.18) and (5.20) ensure that (5.11) and (5.13) can be matched, at leading order, with (5.1) and (5.3). We defer solution of (5.15) and (5.16) until § 5.4.

5.3. *Region III. Downwelling jet*

In the narrow downwelling jet (region III), analogous reasoning suggests that

$$v_x(y,z) \sim \bar{U} + La^{1/2}u_{III}(Y,z), \tag{5.21}$$

$$\psi(y,z) \sim La^{1/2}\psi_{III}(Y,z), \tag{5.22}$$

$$\Omega(y,z) \sim \Omega_{III}(Y,z), \tag{5.23}$$

where $Y \equiv y/La^{1/2}$. Keeping Y, z fixed as $La \to 0$, we obtain the leading-order equations

$$\frac{\partial^2\psi_{III}}{\partial Y^2} = 0 \;\Rightarrow\; \psi_{III}(Y,z) = -W(z)Y, \tag{5.24}$$

$$\frac{\partial^2 u_{III}}{\partial Y^2} = W(z)\frac{\partial u_{III}}{\partial z} - W'(z)Y\frac{\partial u_{III}}{\partial Y}, \tag{5.25}$$

$$\frac{\partial^2\Omega_{III}}{\partial Y^2} = W(z)\frac{\partial\Omega_{III}}{\partial z} - W'(z)Y\frac{\partial\Omega_{III}}{\partial Y} + \frac{\partial u_{III}}{\partial Y}. \tag{5.26}$$

Note that (5.22), (5.24) and (5.8) imply that $\psi(y,z)$ within region III can be matched with the interior solution if $W(z) = w_{II}(0,z)$ (cf. (5.10)). Since $\psi_{III}(Y,z)$ is known apart from the constant $\bar{\Omega}$, the boundary-layer equations (5.25) and (5.26) for $u_{III}(Y,z)$ and $\Omega_{III}(Y,z)$ linearize. Unlike the near-surface boundary layer, however, the vertical vorticity in the downwelling jet is $O(1)$; thus, (5.25) and (5.26) do not fully decouple. These equations must be solved subject to the following boundary conditions:

$$\frac{\partial u_{III}}{\partial Y}(0,z) = 0, \tag{5.27}$$

$$u_{III}(Y,z) \to 0 \quad \text{as } Y \to \infty, \tag{5.28}$$

$$\Omega_{III}(0,z) = 0, \tag{5.29}$$

$$\Omega_{III}(Y,z) \to \bar{\Omega} \quad \text{as } Y \to \infty, \tag{5.30}$$

which ensure that leading-order matching of $v_x(y,z)$ and $\Omega(y,z)$ between the downwelling zone and the vortex core is possible.

5.4. *Region I and III solutions*

To solve for the downwind velocity and vorticity in the surface boundary layer and downwelling jet, the Von Mises coordinate transformation, in which the streamfunction replaces Z and Y as the independent variable in regions I and III, respectively, is used. This transformation has the advantage that it converts the non-constant-coefficient advection–diffusion equations to constant-coefficient diffusion equations following a further transformation of the parabolic coordinate. The new independent coordinates are sometimes referred to as Crocco's variables.

In region I, we set $u_I(y,Z) = U_I(s,\psi_I)$, $V(y) = \mathscr{V}(s)$, where

$$s(y) \equiv \int_{\pi/k}^{y} V(\tau)\,\mathrm{d}\tau = \sum_{n=1}^{\infty}\left(\frac{4\bar{\Omega}}{\pi k^2 n^3}\right)\tanh\left(\frac{nk}{2}\right)\left[1+\cos(nky)\right] \tag{5.31}$$

(the sum is taken over odd n), which converts (5.15) and (5.17)–(5.18) to:

$$\frac{\partial U_I}{\partial s} = \frac{\partial^2 U_I}{\partial \psi_I^2}, \tag{5.32}$$

$$\frac{\partial U_I}{\partial \psi_I}(s, 0) = \frac{1}{\mathscr{V}(s)}, \tag{5.33}$$

$$U_I(s, \psi_I) \to 0 \quad \text{as } \psi_I \to \infty. \tag{5.34}$$

Similarly, setting $\Omega_I(y, Z) = \tilde{\Omega}_I(s, \psi_I) \equiv \bar{\Omega} - \omega_I(s, \psi_I)$ yields:

$$\frac{\partial \omega_I}{\partial s} = \frac{\partial^2 \omega_I}{\partial \psi_I^2}, \tag{5.35}$$

$$\omega_I(s, 0) = \bar{\Omega}, \tag{5.36}$$

$$\omega_I(s, \psi_I) \to 0 \quad \text{as } \psi_I \to \infty. \tag{5.37}$$

In region III, we set $u_{III}(Y, z) = U_{III}(\psi_{III}, r)$, $W(z) = \mathscr{W}(r)$, where

$$r(z) \equiv \int_0^z W(\tau)\,\mathrm{d}\tau = \sum_{n=1}^{\infty} \left(-\frac{4\bar{\Omega}}{\pi k n^2}\right) \left[z + \frac{1 - \mathrm{e}^{nkz} + \mathrm{e}^{-nk(z+1)} - \mathrm{e}^{-nk}}{nk\,(1 + \mathrm{e}^{-nk})}\right] \tag{5.38}$$

(again, the sum is taken over odd n), which converts (5.25) and (5.27)–(5.28) to:

$$\frac{\partial U_{III}}{\partial r} = \frac{\partial^2 U_{III}}{\partial \psi_{III}^2}, \tag{5.39}$$

$$\frac{\partial U_{III}}{\partial \psi_{III}}(0, r) = 0, \tag{5.40}$$

$$U_{III}(\psi_{III}, r) \to 0 \quad \text{as } \psi_{III} \to \infty. \tag{5.41}$$

Finally, setting $\Omega_{III}(Y, z) = \tilde{\Omega}_{III}(\psi_{III}, r) \equiv \bar{\Omega} - \omega_{III}(\psi_{III}, r)$ yields:

$$\frac{\partial \omega_{III}}{\partial r} = \frac{\partial^2 \omega_{III}}{\partial \psi_{III}^2} - \frac{1}{\mathscr{W}(r)} \frac{\partial U_{III}}{\partial \psi_{III}}, \tag{5.42}$$

$$\omega_{III}(0, r) = \bar{\Omega}, \tag{5.43}$$

$$\omega_{III}(\psi_{III}, r) \to 0 \quad \text{as } \psi_{III} \to \infty. \tag{5.44}$$

The solutions to the diffusion problems in region I are standard (see e.g. Carslaw & Jaeger 1959, p.79):

$$U_I(s, \psi_I) = -\frac{1}{\sqrt{\pi}} \int_0^s \frac{\exp\left(-\psi_I^2/4(s - \bar{s})\right)}{\mathscr{V}(\bar{s})\sqrt{s - \bar{s}}}\,\mathrm{d}\bar{s} + \frac{1}{2} \int_0^{\infty} \frac{\mathrm{d}U_{I_0}}{\mathrm{d}\eta}(\eta) \left[\operatorname{erf}\left(\frac{\psi_I - \eta}{2\sqrt{s}}\right) - \operatorname{erf}\left(\frac{\psi_I + \eta}{2\sqrt{s}}\right)\right] \mathrm{d}\eta, \tag{5.45}$$

where $U_{I_0}(\psi_I)$ is the (as yet unknown) profile of $U_I(s, \psi_I)$ as $s \to 0$; and

$$\tilde{\Omega}_I(s, \psi_I) = \bar{\Omega} \operatorname{erf}\left(\frac{\psi_I}{2\sqrt{s}}\right) - \frac{1}{2\sqrt{\pi}\sqrt{s}} \int_0^{\infty} \left(\bar{\Omega} - \tilde{\Omega}_{I_0}(\eta)\right) \times \left[\exp\left(\frac{-(\psi_I - \eta)^2}{4s}\right) - \exp\left(\frac{-(\psi_I + \eta)^2}{4s}\right)\right] \mathrm{d}\eta, \tag{5.46}$$

where $\tilde{\Omega}_{I_0}(\psi_I)$ is the profile of $\tilde{\Omega}_I(s,\psi_I)$ as $s \to 0$. Similarly, the solution to (5.39) and the associated boundary conditions is

$$U_{III}(\psi_{III}, r) = \frac{1}{2}\int_0^\infty \frac{\mathrm{d}U_{III_0}}{\mathrm{d}\eta}(\eta)\left[\mathrm{erf}\left(\frac{\psi_{III}-\eta}{2\sqrt{r}}\right) - \mathrm{erf}\left(\frac{\psi_{III}+\eta}{2\sqrt{r}}\right)\right]\mathrm{d}\eta, \quad (5.47)$$

where $U_{III_0}(\psi_{III})$ is the unknown profile of $U_{III}(\psi_{III}, r)$ as $r \to 0$. Finally, the solution to (5.42) is formally identical (with obvious notational changes) to (5.46) except for the addition of a term of the form $f(r)\partial U_{III}/\partial\psi_{III}$, where

$$f(r) = \int_0^r \frac{\mathrm{d}\bar{r}}{\mathscr{W}(\bar{r})} = z(r),$$

which accounts for the downwind vorticity generated by the Craik–Leibovich vortex force acting within the downwelling zone. Using (5.47),

$$\tilde{\Omega}_{III}(\psi_{III}, r) = \bar{\Omega}\,\mathrm{erf}\left(\frac{\psi_{III}}{2\sqrt{r}}\right) + \frac{1}{2\sqrt{\pi}\sqrt{r}}\int_0^\infty \left[z(r)\frac{\mathrm{d}U_{III_0}}{\mathrm{d}\eta}(\eta) - \left(\bar{\Omega} - \tilde{\Omega}_{III_0}(\eta)\right)\right] \times \left[\exp\left(\frac{-(\psi_{III}-\eta)^2}{4r}\right) - \exp\left(\frac{-(\psi_{III}+\eta)^2}{4r}\right)\right]\mathrm{d}\eta, \quad (5.48)$$

where $\tilde{\Omega}_{III_0}(\psi_{III})$ is the function $\tilde{\Omega}_{III}(\psi_{III}, r)$ as $r \to 0$.

To evaluate (5.45)–(5.48), the unknown 'upstream' profiles of $v_x(y,z)$ and $\Omega(y,z)$ in the near-surface boundary layer and downwelling jet must be determined. This requires consideration of the flow passing through the corner regions in figure 4, as discussed further in the next subsection. The unknown core vorticity also must be determined. We note in passing that, were $\bar{\Omega}$ known, the quadratures (5.45)–(5.48) could be used to generate approximate solutions everywhere in these viscous layers simply by substituting a reasonable functional form for each unknown upstream profile.

5.5. *Region i. Inertial corner region*

The near-surface boundary-layer flow is re-directed into a narrow downwelling jet upon passage through the corner region i, where (as evident in the numerical simulations) the horizontal and vertical length scales are commensurate. The vertical scale in region i must increase relative to that in region I, since the horizontal boundary-layer flow slows as the stagnation point $(y,z) = (0,0)$ is approached. Analysis of (5.4) suggests that $V(y) \sim 2\bar{\Omega}\, y \ln y$ as $y \to 0^+$ and that $W(z) \sim -2\bar{\Omega} z \ln|z|$ as $z \to 0^-$. To match the volume fluxes between the corner and the boundary-layer and downwelling jet, we rescale y and z such that $Y_i \equiv y/La^{1/4}$ and $Z_i \equiv z/La^{1/4}$ (see Childress & Gilbert 1995, pp. 135–136) and consider the limiting process in which Y_i, Z_i remain fixed as $La \to 0$. We also rescale the dependent variables:

$$v_x(y,z) \sim \bar{U} + La^{1/2}u_i(Y_i, Z_i), \quad (5.49)$$

$$\psi(y,z) \sim La^{1/2}[\ln La\, \psi_i^{(0)}(Y_i, Z_i) + \psi_i^{(1)}(Y_i, Z_i)] \equiv La^{1/2}\psi_i(Y_i, Z_i), \quad (5.50)$$

$$\Omega(y,z) \sim \Omega_i(Y_i, Z_i). \quad (5.51)$$

Substituting into (2.1)–(2.3), we find that viscous effects and the CL vortex force are absent at leading order, i.e. that $u_i(Y_i, Z_i) \equiv U_i(\psi_i)$ and $\Omega_i(Y_i, Z_i) \equiv \Gamma_i(\psi_i)$, where the functions $U_i(\psi_i)$ and $\Gamma_i(\psi_i)$ are determined via matching upstream with the flow in region I. Sufficiently close to $(y,z) = (0,0)$, viscous sublayers must arise to accommodate the transformation of the constant-stress boundary condition on $v_x(y,z)$ in the surface boundary layer into a zero-stress symmetry condition in

the downwelling zone, but these are not discussed further here. We comment that experience with other boundary-layer problems also suggests that the flow in the corner is inviscid and passive (see e.g. Lyne 1971; Jimenez & Zufiria 1987; Metcalfe & Pedley 2001). In § 6, we construct an asymptotic estimate for the primary unknown, $\bar{\Omega}$, which controls the strength of the cellular flow. With $\bar{\Omega}$ known, the specification of $v_x(y, z)$ (and subsequently $\Omega(y, z)$) in the boundary layers and up- and downwelling jets can be completed by formulating and solving a 'Childress-like' cell problem (see Childress 1979). As discussed in § 7, this computation can be effected without performing a detailed analysis of the viscous corner sublayers, and relies only on the passive advection of $v_x(y, z)$ and $\Omega(y, z)$ through the outer (inertial) corner regions.

6. Determination of the core vorticity

To determine $\bar{\Omega}$, we again make use of certain integral constraints. The first is obtained by multiplying the vorticity equation (2.2) by ψ and integrating over the area of the cell. The advection terms drop out, leaving the following exact result:

$$La \int_{-1}^{0} \int_{0}^{\pi/k} \Omega^2 \, \mathrm{d}y \, \mathrm{d}z = - \int_{-1}^{0} \int_{0}^{\pi/k} \psi \frac{\partial v_x}{\partial y} \, \mathrm{d}y \, \mathrm{d}z. \tag{6.1}$$

Equation (6.1), which also can be derived by taking the inner product of the cellular (i.e. y–z) velocity vector with the momentum equation and integrating over the domain, expresses global energy conservation: the work done by the CL vortex (or buoyancy) torque is balanced by the viscous dissipation of energy, since there is no net flux of energy into or out of the cell. Noting that the area of the cell is π/k, the leading contribution to the term on the left-hand side is $La\bar{\Omega}^2\pi/k$. Since $\partial v_x/\partial y = O(1)$ in the up- and downwelling zones, the area of which is $O(La^{1/2})$ and in which $\psi = O(La^{1/2})$, the dominant contribution to the right-hand side of (6.1) arises in those subdomains and is also $O(La)$. Exploiting the symmetry of the up- and downwelling zones, (6.1) at leading order in La therefore reduces to

$$\begin{aligned}
\bar{\Omega}^2 &\sim -\frac{2k}{\pi} \int_{-1}^{0} \int_{0}^{\infty} \psi_{III} \frac{\partial u_{III}}{\partial Y} \, \mathrm{d}Y \mathrm{d}z, \\
&= -\frac{2k}{\pi} \int_{-1}^{0} \int_{0}^{\infty} \psi_{III} \frac{\partial U_{III}}{\partial \psi_{III}} \, \mathrm{d}\psi_{III} \, \mathrm{d}z, \\
&= -\frac{2k}{\pi} \int_{-1}^{0} \left[\psi_{III} U_{III} \Big|_{0}^{\infty} - \int_{0}^{\infty} U_{III} \, \mathrm{d}\psi_{III} \right] \mathrm{d}z, \\
&= \frac{2k}{\pi} \int_{-1}^{0} \int_{0}^{\infty} U_{III} \, \mathrm{d}\psi_{III} \, \mathrm{d}z,
\end{aligned} \tag{6.2}$$

using the boundary and matching conditions on ψ_{III} and U_{III}.

It would appear that evaluation of the integral arising in (6.2) requires $U_{III}(\psi_{III}, r(z))$ to be completely specified. In fact, this integral can be computed asymptotically by employing (4.2), a second global constraint: in steady state, the convection zone is a constant (downwind-momentum or heat) flux layer. As $La \to 0$, the exact relation (4.2) can be approximated asymptotically as:

$$\frac{\pi}{2k} \sim -W(z) \int_{0}^{\infty} u_{III}(Y, z) \, \mathrm{d}Y = \int_{0}^{\infty} U_{III}(\psi_{III}, r) \, \mathrm{d}\psi_{III}. \tag{6.3}$$

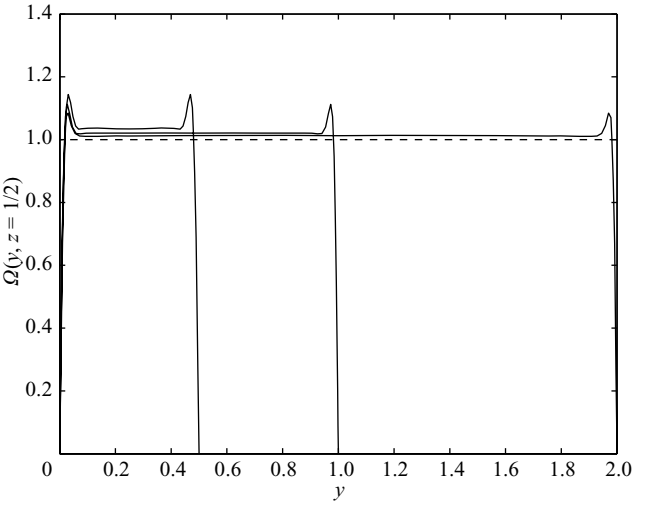

FIGURE 5. Steady-state solutions computed numerically for $La = 0.0001$ for three different cell aspect ratios. The plots show the core vorticity at the cell mid-plane as a function of the cross-wind coordinate y and confirm that $\bar{\Omega} \sim 1$ independently of k as $La \to 0$.

Note that this result is valid for any $\bar{\Omega}$. With the streamfunction expressed as $\psi(y, z) = \bar{\Omega}\Psi(y, z)$ for some given function $\Psi(y, z)$ satisfying the boundary conditions on ψ around the cell perimeter, (2.1) is linear and (4.2) (and hence (6.3)) is merely a solvability condition on $v_x(y, z)$ for the given streamfunction. However, by substituting (6.3) into (6.2), the following simple result is obtained:

$$\bar{\Omega}^2 \sim 1 \;\Rightarrow\; \bar{\Omega} \sim \pm 1. \tag{6.4}$$

The sign of $\bar{\Omega}$ determines the sense of the cellular flow; for consistency with figure 4, we select the positive root. We emphasize that (6.4) is not a mere order-of-magnitude estimate but, rather, a precise asymptotic result which indicates that the finite 'amplitude' of the vortex motion, $\bar{\Omega}$, is independent of the cell wavenumber k. To test this somewhat surprising prediction, the pseudospectral algorithm described in § 3 was modified by using a Chebyshev–Chebyshev (rather than Fourier–Chebyshev) 'tensor-product' grid (Trefethen 2000) and lateral symmetry conditions (2.6) to provide adequate resolution of the boundary layers and up- and downwelling jets. To further improve the resolution of the viscous layers, a tensor-product rational mapping was employed for certain computations. In all cases, a minimum of ten grid points was used to resolve the viscous layers. Solutions were computed for $La = 0.0001$ for three different values of k. As evident in figure 5, all solutions exhibit a nearly constant core vorticity with a value close to unity in each case, confirming the asymptotic prediction (6.4).

7. A Childress-like cell problem

Having determined $\bar{\Omega}$, we can compute $v_x(y, z)$ in the boundary layers and up- and downwelling zones without carrying out detailed matching of the flow fields through the viscous corner sublayers (to determine the unknown profiles arising in (5.45) and (5.47)) by formulating a 'Childress-like' cell problem (see Childress 1979). In particular, we exploit the fact that in the outer (inviscid) corner subdomains, U is

passively advected between the boundary layers and plumes (as shown in § 5.5), where U and ψ with subscripts omitted here refer to the corresponding region I or III scaled variables, and the 'time-like' coordinates s and r are replaced with the single variable ξ which runs around the perimeter of the cell. In the small-La limit, the corner domains have dimensions that are small compared with the streamwise extent of the boundary layers and plumes. Thus, as a function of ξ and ψ, U satisfies a simple diffusion equation around the entire cell perimeter subject to specified flux boundary conditions and a periodicity rather than initial condition in the ξ coordinate. At the 'points' joining the boundary layers and plumes, U is continuous except, possibly, at $\psi = 0$, where the boundary conditions require a discontinuity in $\partial U/\partial\psi$ and may cause a discontinuity in U itself. The resulting cell problem is similar to that formulated by Childress (1979), Roberts (1979), Jimenez & Zufiria (1987) and Soward (1987), but: (i) arises here as the solution to a fully nonlinear problem (i.e. for unit rather than infinite Prandtl number); and (ii) does not give rise to an integral equation and, in fact, can be solved explicitly (e.g. without recourse to the Wiener–Hopf method).

Making use of the result $\bar{\Omega} \sim 1$, we thus have the following algorithm for determining U.

(*a*) Solve $\nabla^2\psi_{II} = -1$ on $0 \leqslant y \leqslant \pi/k$, $-1 \leqslant z \leqslant 0$ with $\psi_{II} = 0$ boundary conditions.

(*b*) Obtain $V(y)$, $W(z)$, $s(y)$, $r(z)$ from the solution to (*a*).

(*c*) Compute the lengths of the near-surface boundary layer $l_1 \equiv s(0)$ and downwelling zone $l_2 \equiv r(-1)$ in the s and r coordinates. Define $l \equiv 2l_1 + 2l_2$, the cell perimeter in these units.

(*d*) Solve the diffusion equation $\partial U/\partial\xi = \partial^2 U/\partial\psi^2$, where $0 \leqslant \psi < \infty$, $0 < \xi < l$, subject to

$$\begin{aligned}
&\frac{\partial U}{\partial\psi} = F(\xi) = \frac{1}{\mathscr{V}(\xi)} \quad (0 \leqslant \xi < l_1),\\
&\frac{\partial U}{\partial\psi} = F(\xi) = 0 \quad (l_1 \leqslant \xi < l_1 + l_2),\\
&\frac{\partial U}{\partial\psi} = F(\xi) = -\frac{1}{\mathscr{V}(\xi - l_1 - l_2)} \quad (l_1 + l_2 \leqslant \xi < 2l_1 + l_2),\\
&\frac{\partial U}{\partial\psi} = F(\xi) = 0 \quad (2l_1 + l_2 \leqslant \xi < l),
\end{aligned}$$

at $\psi = 0$; the far-field condition $U(\xi, \psi) \to 0$ as $\psi \to \infty$; and the periodicity constraint

$$U(\xi + nl, \psi) = U(\xi, \psi) \qquad (n = 1, 2, 3\ldots).$$

Referring to (5.45), the formal solution to this problem can be expressed as

$$\begin{aligned}
U(\xi, \psi) = &-\frac{1}{\sqrt{\pi}} \int_0^{\xi} F(\xi - p)\, \frac{\mathrm{e}^{(-\psi^2/4p)}}{\sqrt{p}}\, \mathrm{d}p\\
&+ \frac{1}{2} \int_0^{\infty} \frac{\mathrm{d}U_0}{\mathrm{d}\eta}(\eta) \left[\mathrm{erf}\left(\frac{\psi - \eta}{2\sqrt{\xi}}\right) - \mathrm{erf}\left(\frac{\psi + \eta}{2\sqrt{\xi}}\right)\right] \mathrm{d}\eta. \quad (7.1)
\end{aligned}$$

To avoid iterating to determine $U_0(\psi)$, the unknown profile of $U(\xi, \psi)$ at $\xi = 0$, we follow Jimenez & Zufiria (1987) by re-expressing (7.1) exploiting the periodicity of

$U(\xi, \psi)$:

$$U(\xi,\psi) = -\frac{1}{\sqrt{\pi}}\int_0^{\xi+nl} F(\xi+nl-p)\,\frac{\mathrm{e}^{(-\psi^2/4p)}}{\sqrt{p}}\,\mathrm{d}p + \frac{1}{2}\int_0^{\infty}\frac{\mathrm{d}U_0}{\mathrm{d}\eta}(\eta)\left[\mathrm{erf}\left(\frac{\psi-\eta}{2\sqrt{\xi+nl}}\right)-\mathrm{erf}\left(\frac{\psi+\eta}{2\sqrt{\xi+nl}}\right)\right]\mathrm{d}\eta.$$

Taking the limit as $n \to \infty$, the second integral vanishes, and observing that $F(\xi)$ is also nl-periodic then yields

$$\begin{aligned} U(\xi,\psi) &= -\frac{1}{\sqrt{\pi}}\int_0^{\infty} F(\xi-p)\,\frac{\mathrm{e}^{(-\psi^2/4p)}}{\sqrt{p}}\,\mathrm{d}p \\ &= -\frac{1}{\sqrt{\pi}}\int_0^{\xi}[\cdot]\,\mathrm{d}p - \frac{1}{\sqrt{\pi}}\int_{\xi}^{\infty}[\cdot]\,\mathrm{d}p \\ &\equiv I_1 + I_2, \end{aligned} \tag{7.2}$$

where we split the integral into two contributions for computational convenience. The first integral can be expressed as

$$I_1 = -\frac{1}{\sqrt{\pi}}\int_0^{\xi} F(s)\,\frac{\mathrm{e}^{(-\psi^2/4(\xi-s))}}{\sqrt{\xi-s}}\,\mathrm{d}s,$$

and, recalling that $\mathrm{d}s/\mathscr{V}(s) = \mathrm{d}y$, if e.g. ξ is in the downwelling zone ($l_1 < \xi < l_2$),

$$I_1 = \frac{1}{\sqrt{\pi}}\int_0^{\pi/k}\frac{\mathrm{e}^{(-\psi^2/4(\xi-s(y)))}}{\sqrt{\xi-s(y)}}\,\mathrm{d}y,$$

where I_1 can be evaluated without special precautions. Again for computational convenience, I_2 can be rewritten as an infinite sum of integrals around the cell perimeter (Jimenez & Zufiria 1987):

$$\begin{aligned} I_2 &= \sum_{n=1}^{\infty}\left[-\frac{1}{\sqrt{\pi}}\int_0^{l} F(\mu)\,\frac{\mathrm{e}^{(-\psi^2/4(\xi-\mu+nl))}}{\sqrt{\xi-\mu+nl}}\right]\mathrm{d}\mu \\ &= \sum_{n=1}^{\infty}\frac{1}{\sqrt{\pi}}\int_0^{l_1}\frac{1}{\mathscr{V}(s)}\left[\frac{\mathrm{e}^{(-\psi^2/4(\xi-s-l_1-l_2+nl))}}{\sqrt{\xi-s-l_1-l_2+nl}}-\frac{\mathrm{e}^{(-\psi^2/4(\xi-s+nl))}}{\sqrt{\xi-s+nl}}\right]\mathrm{d}s \\ &= \sum_{n=1}^{\infty}-\frac{1}{\sqrt{\pi}}\int_0^{\pi/k}\left[\frac{\mathrm{e}^{(-\psi^2/4(\xi-s(y)-l_1-l_2+nl))}}{\sqrt{\xi-s(y)-l_1-l_2+nl}}-\frac{\mathrm{e}^{(-\psi^2/4(\xi-s(y)+nl))}}{\sqrt{\xi-s(y)+nl}}\right]\mathrm{d}y, \end{aligned}$$

where we note that for large n, ψ fixed and $O(1)$, the term in $[\cdot] \sim (l_1+l_2)/(2l^{3/2}n^{3/2})$.

In figure 6, the asymptotic solution for $v_x(y, -1/2)$, computed by numerically evaluating the quadratures defining I_1 and I_2 and reconstructing v_x for $La = 0.0001$ and $k = 2\pi$, is compared to the corresponding steady-state numerical solution obtained using the Chebyshev–Chebyshev pseudospectral code. The quantitative agreement between the two solutions is satisfactory given that the fully analytical solution has no adjustable coefficients and that the chosen value of La, although small compared to unity, is necessarily finite. Indeed, the discrepancy between the two solutions is consistent with $O(La|\ln La|)$ corrections to the leading-order asymptotic

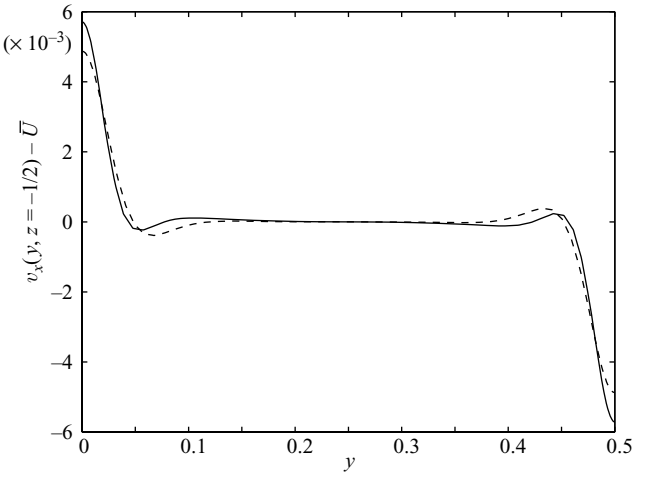

FIGURE 6. Comparison of the analytical (dashed) and steady-state numerical (solid) solutions for $v_x(y, z)$ at $La = 0.0001$ and $k = 2\pi$.

expansion of $v_x(y, z) - \bar{U}$ arising in the viscous layers, as is suggested by a preliminary higher-order matching analysis between the corner and the boundary layer and downwelling zone. The Childress solution for $v_x(y, z)$ at a given location within the downwelling zone (e.g. at the mid-depth $z = -1/2$) can be used to evaluate the left-hand side of (5.47), enabling the unknown profile $\mathrm{d}U_{III_0}(\eta)/\mathrm{d}\eta$ to be determined by Fourier cosine transforming both sides of the equation. Although not pursued here, the result can be substituted into (5.48), and then (5.46) and (5.48) can be equated at $(s(0), r = 0)$ and $(s = 0, r(-1))$ to determine $\tilde{\Omega}_{I_0}(\eta)$ and $\tilde{\Omega}_{III_0}(\eta)$; note that there is no discontinuity in the imposed boundary conditions on $\Omega(y, z)$ along the edge of the cell as the corners are traversed. Thus, in principle, $\Omega(y, z)$ also can be completely determined by this asymptotic analysis.

8. Hybrid analytical–computational method

A simple approximate hybrid analytical–computational solution for $v_x(y, z)$ can be obtained by substituting the analytically determined streamfunction given in (5.5) and (5.6), with $\bar{\Omega} \equiv 1$, into the downwind momentum equation (2.1) and solving the resulting equation numerically. This approach has the advantage that it avoids the analytical complexities of the asymptotic solution for v_x while requiring only a single numerical inversion of a suitably discretized linear differential operator; in contrast, a full numerical computation of $v_x(y, z)$ requires that the fully coupled nonlinear system of equations (2.1)–(2.3) be solved iteratively or by advancing the corresponding time-dependent system to steady state. Compared to these alternatives, the hybrid approach is significantly easier to program, has more modest computational memory requirements and requires much less computing time (see below). With $v_x(y, z)$ obtained using the hybrid algorithm, the result can be substituted into (2.2) and the same method used to calculate $\Omega(y, z)$. The key observation is that, as $La \to 0$, the analytical solution for $\psi_{II}(y, z)$ provides a good approximation to $\psi(y, z)$ and its first spatial derivatives with respect to y and z, i.e. to $v(y, z)$ and $w(y, z)$, over the entire domain: unlike $\Omega(y, z)$ and $v_x(y, z)$, $\psi(y, z)$ does not exhibit regions of sharp gradients (see figure 1). This specification reduces (2.1) to a linear advection–diffusion equation.

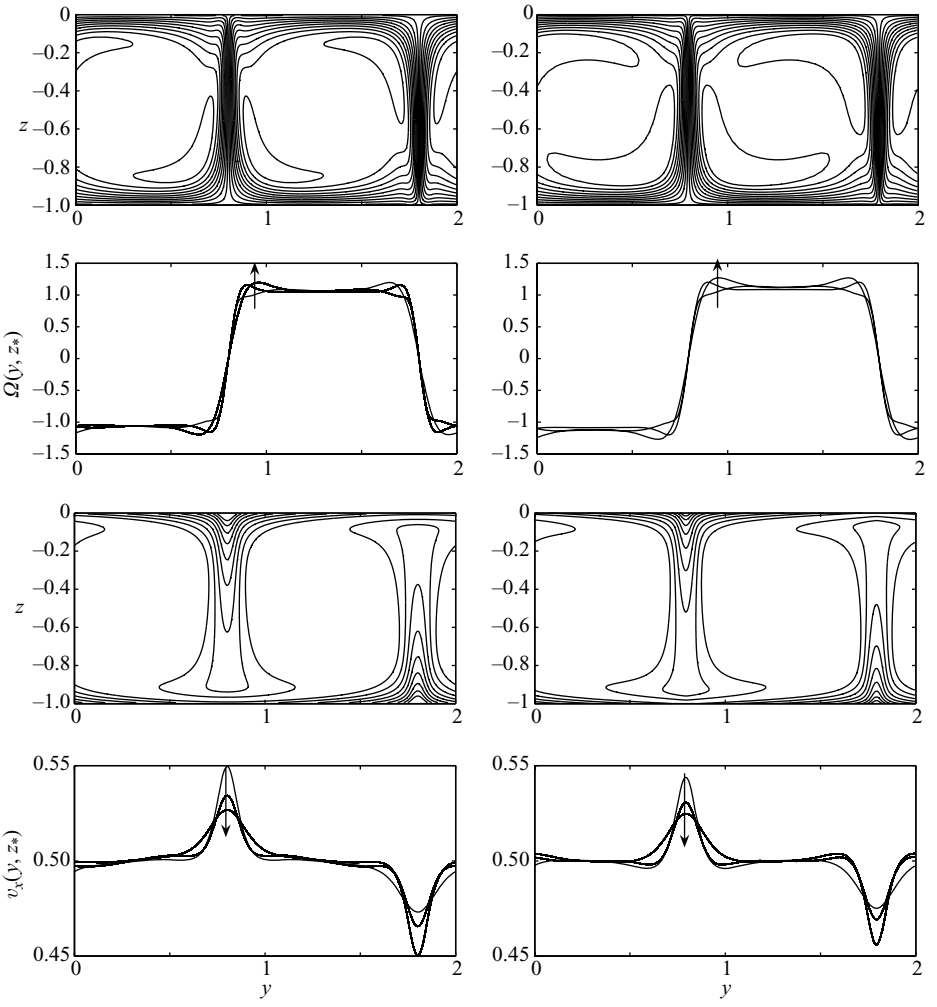

FIGURE 7. Comparison of the full numerical (left) and hybrid analytical–computational (right) solutions for $\Omega(y,z)$ and $v_x(y,z)$ for $La = 0.0012$ and $k = \pi$. The upper plots show the steady vorticity field $\Omega(y,z)$. The lower plots show the total downwind velocity (or temperature) field $v_x(y,z)$. Contour levels are identical to those in figures 2 and 3, respectively. In the plots of $v_x(y,z_*)$ versus y, the arrows indicate the direction of decreasing z_* (increasing depth), with the uppermost curve corresponding to $z_* = -1/4$, the middle curve to $z_* = -1/2$ and the lowest curve to $z_* = -3/4$. The hybrid solutions were computed by numerically solving (2.1) and (2.2) subject to cell boundary conditions (2.5) and (2.6) using the *analytically-determined* streamfunction given in (5.5) and (5.6) with $\bar{\Omega} \equiv 1$.

Figure 7 shows the close quantitative agreement between the semi-analytical and full numerical solutions for $\Omega(y,z)$ and $v_x(y,z)$ for the relatively modest value of $La = 0.0012$. While the full numerical simulations required $O(10)$ hours (on a Pentium M 1.86 GHz processor), the hybrid analytical–numerical solutions required less than one minute to compute.

9. Conclusion

We have used a complement of asymptotic analysis and well-resolved pseudo-spectral numerical simulations to elucidate the structure of steady two-dimensional

Langmuir circulation and Rayleigh–Bénard convection in the weak-dissipation/strong-forcing limit (i.e. as $La \to 0$, or $Ra \to \infty$ at unit Prandtl number). Our analysis extends earlier studies of large Rayleigh-number, infinite Prandtl-number thermal convection, and related investigations of passive scalar transport and flux expulsion by eddies, in which the cellular flow satisfies a linearized momentum equation or is prescribed. In contrast, here the full nonlinear momentum equation is treated: the vorticity in the core of the cell is dominated by nonlinear inertial rather than linear viscous effects and, in steady state, approaches a uniform value $\bar{\Omega}$.

A central result of the asymptotic analysis is that $|\bar{\Omega}| \sim 1$ as $La \to 0$, independently of the cell aspect ratio. This result follows from the homogenization of $\Omega(y, z)$ and $v_x(y, z)$ – the temperature in Rayleigh–Bénard convection or the downwind velocity in Langmuir circulation – in the vortex core and from two integral constraints. A global energy budget reveals that the dominant contribution to the $O(La)$ work done by the buoyancy or CL vortex torque arises in narrow up- and downwelling zones of thickness $O(La^{1/2})$, while the dominant contribution to the viscous dissipation of kinetic energy occurs in the vortex core (not in the corners as speculated by Moore & Weiss 1973). Although the core behaves as a dynamically inviscid region, the $O(La)$ energy dissipation in the core dominates that in the boundary layers. This slightly counter-intuitive result is well-known in the context of free-surface boundary layers (see Batchelor 1967, p. 367), where the primary contribution to the volume-integrated energy dissipation is induced by irrotational straining outside of the boundary layer. For the convective states investigated here, the flow in the core has uniform vorticity, but the streamlines are not strictly circular, and fluid elements are subjected to significant straining as they translate and rotate. The picture that emerges is that the kinetic energy produced in the up- and downwelling zones is advected around the corners to the top and bottom boundary layers; simultaneously, there is an $O(La)$ diffusive transport of kinetic energy between the viscous layers and the vortex core, where the mechanical energy is dissipated.

A second global constraint is that the steady-state convection zone is a constant heat (or downwind-momentum) flux layer. For the solutions investigated, the conductive flux across the upper and lower horizontal boundaries is entirely carried by the narrow plumes, away from the thin top and bottom boundary layers. In this investigation, the flux is prescribed; thus, the horizontal integral of this flux scales in direct proportion to the cell width π/k. Since the work done within the plumes can be expressed in terms of this horizontally integrated flux (see (6.2) and (6.3)), the work also scales in direct proportion to π/k; so, too, does the energy dissipation, which scales with the area of the cell (π/k) since most of the dissipation occurs in the core where $\Omega(y, z)$ is uniform. Thus, asymptotically, $\bar{\Omega}$ is independent of the horizontal wavenumber k, as corroborated by the numerical simulations.

A final noteworthy aspect of the asymptotic vortex structure is that, given stress-free conditions on the cellular flow, the streamfunction is smooth in the weak-diffusion limit even though the associated vorticity is not. Consequently, the advection–diffusion equations for $v_x(y, z)$ and $\Omega(y, z)$ linearize in the viscous layers surrounding the vortex core, enabling the solution to the full nonlinear boundary-value problem to be reduced to quadratures. We emphasize that the analytical solutions obtained here are fully nonlinear in that the vortices are sufficiently strong to completely restructure the linear downwind-velocity (or, for thermal convection, temperature) profile realized in the absence of convection. Thus, our approach complements the more usual weakly nonlinear convection analyses in which the basic-state profiles are not altered at leading order by the presence of the convection cells.

It is interesting to briefly compare our small-La analysis with two other finite-amplitude convection theories, which are based on long-wavelength and 'modal' approximations, respectively. Exploiting the fact that $k_c = 0$ when constant-flux boundary conditions are imposed, Cox & Leibovich (1993) derived a 'fully' nonlinear reduced model of long-wavelength (i.e. small k) LC that is valid sufficiently close to the onset of convection. In their theory, the downwind velocity perturbation $u(y, z)$ to the basic-state shear flow $U_b(z)$ is allowed to be $O(1)$. As indicated in § 1, however, the basic-state shear flow gradient is not modified at leading-order in k since the $O(1)$ downwind velocity perturbation is depth-independent. Moreover, the cellular flow is weak, being characterized by $O(k)$ horizontal velocities and $O(k)$ non-uniform downwind vorticity. As $k \to 0$, the small-La convective states, which are valid far from the primary instability threshold, do not approach these solutions. Indeed, in this limit, the small-La solutions feature $O(1)$ depth-varying downwind velocity perturbations and $O(1)$ cross-wind horizontal velocities, so the downwind velocity and $O(1)$ downwind vorticity remain spatially uniform in each vortex core. Furthermore, an examination of the behaviour of solutions to the Poisson equation (5.4) as $k \to 0$ reveals that the vertical velocity vanishes in the core, but reaches $O(1)$ values near the up- and downwelling zones; in contrast, the small-k finite-La convective states exhibit $O(k^2)$ vertical velocities throughout the domain.

At finite k, the small-La analytical solution for the streamfunction obtained in § 5 lends some support to the single-mode convection approximation of Gough *et al.* (1975), since (5.5) and (5.6) show that $\psi(y, z)$ is dominated by its lowest Fourier mode. In their approximation scheme, the horizontal (but not vertical) structure of each dependent variable is expanded in a series of orthogonal functions; Galerkin projection of the governing equations is then employed, followed by a severe truncation in which only a single horizontal mode is retained. While the present analysis suggests that this truncation may be a reasonable approximation for the streamfunction and its first spatial derivatives (i.e. the cellular velocity components), the (x) vorticity and temperature fields clearly cannot be accurately approximated by retaining only a single or even a small number of Fourier modes.

An obvious question not investigated here concerns the stability of the strongly nonlinear asymptotic solutions. Indeed, for sufficiently small La, the steady cellular solutions are expected to be unstable to small-scale disturbances. The numerical simulations suggest that – in two-dimensions – these instabilities do not occur for $La \geqslant O(10^{-4})$, i.e. values of La that may be of oceanographic relevance. Importantly, both the full asymptotic and, particularly, the hybrid analytical–computational solutions show good agreement with the steady-state numerical solutions for $10^{-4} \leqslant La \leqslant 10^{-3}$. If the evolution is laminar, the time required to attain these steady states is proportional to the diffusion time scale H^2/ν_e (cf. Rhines & Young 1983). If $La \ll O(10^{-4})$, the evolution is likely to be turbulent. Our conjecture is that the laminar solutions investigated here may nevertheless play some role in the turbulent dynamics, acting as a saddle on a high-dimensional attractor, in which case the time required to visit the neighbourhood of these solutions could be much less than the laminar diffusive time scale. If valid, this conjecture is more likely to be relevant for Langmuir circulation than for thermal convection, since observations, simulations and theory support the view that quasi-two-dimensional vortices elongated in the wind direction are preferred. We note that the downwind- and time-averaged downwind velocity profiles extracted from the large-eddy simulations of turbulent Langmuir circulation by Tejada-Martinez & Grosch (2007) exhibit a striking qualitative resemblance to the laminar solutions analysed here. (Specifically, compare their figures 3*a* and 8*a* with

figures 3*a* and 3*b* of the present work, and note that Tejada-Martinez & Grosch employ a no-slip lower boundary condition and an exponentially decaying Stokes drift.) Perhaps similar considerations would apply for Rayleigh–Bénard convection in a shear flow, where again, roll vortices aligned with the shear control the dynamics and transport. Moreover, Newell, Rand & Russell (1988) put forth the intriguing conjecture that turbulent transport may be dominated by the random occurrence of coherent events that these authors contend are closely related to solutions of the governing equations in the weak-dissipation limit. Newell *et al.* identify thermal convection at large Rayleigh numbers, in which transport is dominated by narrow plumes, as one apt candidate for the theory they espouse. Of course, comparisons with direct numerical simulations of 'Langmuir turbulence' and turbulent thermal convection are required to test this conjecture in the present context.

Given these considerations, one useful extension of the present work would be to carry out a quasi-inviscid secondary stability analysis to investigate the way in which the steady two-dimensional asymptotic solutions break down into turbulence. A related line of investigation concerns the modulational stability of the steady cellular solutions, i.e. their stability to disturbances having a length scale much greater than the cell width (Novikov & Papanicolaou 2001). To this end, the quasi-linearization of the governing equations afforded by analytical knowledge of the cellular streamfunction should facilitate the required homogenization analysis. We are pursuing a third extension by adapting the analysis described here to treat Rayleigh–Bénard convection with the more usual specified temperature rather than specified heat-flux conditions. The corresponding large-Ra convection solutions exhibit a classically proposed relationship between the Nusselt number Nu (a non-dimensional measure of the heat flux through the layer) and Rayleigh number; namely, $Nu \sim CRa^{1/3}$, where the $O(1)$ coefficient C can be shown to depend on the wavenumber of the convection pattern but not on the Prandtl number, for the given stress-free boundary conditions. This analysis will be reported elsewhere. The highly nonlinear convective states obtained in the present study necessarily are constant-flux solutions, for which a satisfactory definition of an appropriate Nusselt number is less obvious. Otero *et al.* (2002) show that the conventional definition of the Nusselt number requires, for constant heat-flux convection, $Nu = 1/|\Delta v_x| = 1/|\Delta T|$, where ΔT refers to the (non-dimensional) horizontal-mean temperature difference between $z = 0$ and $z = -1$. (This definition is also physically appealing since intense convection largely eradicates the temperature difference across the layer.) With this choice, our solutions satisfy $Nu \sim C(k)Ra^{1/3}$ as $Ra \to \infty$ (or, equivalently, $Nu \sim C(k)La^{-1/2}$ as $La \to 0$), again independently of Prandtl number, as for the case of Dirichlet boundary conditions. Our scaling estimate satisfies the rigorous bound for constant heat-flux RBC obtained by Otero *et al.* (2002), which requires $Nu \leqslant \tilde{c}Ra^{1/2}$ for an $O(1)$ constant $\tilde{c}$, and more closely agrees with experimental data for finite-Prandtl-number convection.

In the Langmuir circulation context, the small-La analysis may be modified to incorporate more realistic exponentially (rather than linearly) decaying Stokes drift profiles. This extension is challenging, since the discrete rotational symmetry possessed by the solutions investigated here is broken. Finally, the results of the present investigation suggest certain useful guidelines for simulations of unsteady convection at small La: specifically, the vorticity field exhibits passive boundary layers, which need not be resolved; and the streamfunction does not exhibit boundary or internal layers, and hence may be resolved with a modicum of modes. These various extensions are the subject of future work.

G. P. C. benefited greatly from discussions with Bill Young, Stefan Llewellyn Smith and Steve Childress during a WHOI GFD Summer Program and during a visit to UCSD/SIO. The comments of the referees also helped to improve the exposition. G. P. C. gratefully acknowledges funding for this work from NSF CAREER Award 0348981 administered by the Physical Oceanography Program.

REFERENCES

Bassom, A. P. & Zhang, K. 1994 Stongly nonlinear convection cells in a rapidly rotating fluid layer. *J. Geophys. Astrophys. Fluid Dyn.* **76**, 223–238.

Batchelor, G. K. 1956 On steady laminar flow with closed streamlines at large Reynolds number. *J. Fluid Mech.* **1**, 177–190.

Batchelor, G. K. 1967 *An Introduction to Fluid Dynamics*, 1st edn. Cambridge University Press.

Blennerhassett, P. J. & Bassom, A. P. 1991 Stongly nonlinear vortices in Bénard convection. *IMA J. Appl. Maths* **46**.

Busse, F. H. & Clever, R. M. 1981 An asymptotic model of two-dimensional convection in the limit of low Prandtl number. *J. Fluid Mech.* **102**, 75–83.

Caillol, P. & Grimshaw, R. 2004 Steady multipolar planar vortices with nonlinear critical layers. *J. Geophys. Astrophys. Fluid Dyn.* **98**, 473–506.

Carslaw, H. S. & Jaeger, J. C. 1959 *Conduction of Heat in Solids*, 1st edn. Oxford University Press.

Chapman, C. J. & Proctor, M. R. E. 1980 Nonlinear Rayleigh–Bénard convection between poorly conducting boundaries. *J. Fluid Mech.* **101**, 759–782.

Childress, S. 1979 Alpha-effect in flux ropes and sheets. *Phys. Earth Planet. Inter.* **20**, 172–180.

Childress, S. & Gilbert, A. 1995 *Stretch, Twist and Fold: The Fast Dynamo*. Lecture Notes in Physics. Springer.

Cox, S. M. & Leibovich, S. 1993 Langmuir circulations in a surface layer bounded by a strong thermocline. *J. Phys. Oceanogr.* **23**, 1330–1345.

Cox, S. M. & Leibovich, S. 1994 Large-scale Langmuir circulation and double-diffusive convection: evolution equations and flow transitions. *J. Fluid Mech.* **276**, 189–210.

Cox, S. M. & Leibovich, S. 1997 Large-scale three-dimensional Langmuir circulation. *Phys. Fluids* **9**, 2851–2863.

Craik, A. D. D. 1977 The generation of Langmuir circulations by an instability mechanism. *J. Fluid Mech.* **81**, 209–223.

Craik, A. D. D. & Leibovich, S. 1976 A rational model for Langmuir circulations. *J. Fluid Mech.* **73**, 401–426.

Deardorff, J. W. & Willis, G. E. 1967 Investigation of turbulent thermal convection between horizontal plates. *J. Fluid Mech.* **28**, 675–704.

Faisst, H. & Eckhardt, B. 2003 Traveling waves in pipe flow. *Phys. Rev. Lett.* **91**, 224502.

Faisst, H. & Eckhardt, B. 2004 Sensitive dependence on initial conditions in transition to turbulence in pipe flow. *J. Fluid Mech.* **504**, 343–352.

Gough, D. O., Spiegel, E. A. & Toomre, J. 1975 Modal equations for cellular convection. *J. Fluid Mech.* **68**, 695–719.

Jimenez, J. & Zufiria, J. A. 1987 A boundary-layer analysis of Rayleigh–Bénard convection at large Rayleigh number. *J. Fluid Mech.* **178**, 53–71.

Julien, K. & Knobloch, E. 1997 Fully nonlinear oscillatory convection in a rotating layer. *Phys. Fluids* **9**, 1906–1913.

Kawahara, G. & Kida, S. 2001 Periodic motion embedded in plane Couette turbulence: regeneration cycle and burst. *J. Fluid Mech.* **449**, 291–300.

Kerswell, R. R., Tutty, O. R. & Drazin, P. G. 2004 Steady nonlinear waves in diverging channel flow. *J. Fluid Mech.* **501**, 231–250.

Kim, S.-C. 1998 On Prandtl–Batchelor theory of a cylindrical eddy: asymptotic study. *SIAM J. Appl. Maths* **58**, 1394–1413.

Kim, S.-C. & Childress, S. 2001 Vorticity selection with multiple eddies in two-dimensional steady flow at high Reynolds number. *SIAM J. Appl. Maths* **61**, 1605–1617.

Leibovich, S. 1977 On the evolution of the system of wind drift currents and Langmuir circulations in the ocean. Part 1. Theory and averaged current. *J. Fluid Mech.* **79**, 715–743.

Leibovich, S. 1980 On wave–current interaction theories of Langmuir circulations. *J. Fluid Mech.* **99**, 715–724.

Leibovich, S. 1983 The form and dynamics of Langmuir circulations. *Annu. Rev. Fluid Mech.* **15**, 391–427.

Li, M. & Garrett, C. 1993 Cell merging and the jet/downwelling ratio in Langmuir circulation. *J. Mar. Res.* **51**, 737–769.

Lingevitch, J. F. & Bernoff, A. J. 1994 Advection of a passive scalar by a vortex couple in the small-diffusion limit. *J. Fluid Mech.* **270**, 219–249.

Lyne, W. H. 1971 Unsteady viscous flow in a curved pipe. *J. Fluid Mech.* **45**, 13–31.

Mamun, C. K. & Tuckerman, L. S. 1995 Asymmetry and Hopf bifurcation in spherical Couette flow. *Phys. Fluids* **7**, 80–91.

Maslowe, S. A. 1986 Critical layers in shear flows. *Annu. Rev. Fluid Mech.* **18**, 405–432.

Matthews, P. C. 1999 Asymptotic solutions for nonlinear magnetoconvection. *J. Fluid Mech.* **387**, 397–409.

McWilliams, J. C., Sullivan, P. P. & Moeng, C. 1997 Langmuir turbulence in the ocean. *J. Fluid Mech.* **334**, 1–30.

Metcalfe, A. M. & Pedley, T. J. 2001 Falling plumes in bacterial bioconvection. *J. Fluid Mech.* **445**, 121–149.

Moore, D. R. & Weiss, N. O. 1973 Two-dimensional Rayleigh–Bénard convection. *J. Fluid Mech.* **58**, 289–312.

Nagata, M. 1990 Three-dimensional finite-amplitude solutions in plane Couette flow: bifurcation from infinity. *J. Fluid Mech.* **217**, 519–527.

Newell, A. C., Rand, D. A. & Russell, D. 1988 Turbulent transport and the random occurrence of coherent events. *Physica* D **33**, 281–303.

Newell, A. C., Passot, T. & Souli, M. 1990 The phase diffusion and mean drift equations for convection at finite Rayleigh numbers in large containers. *J. Fluid Mech.* **220**, 187–252.

Novikov, A. & Papanicolaou, G. 2001 Eddy viscosity of cellular flows. *J. Fluid Mech.* **446**, 173–198.

Olson, P. & Corcos, G. M. 1980 A boundary layer model for mantle convection with surface plates. *Geophys. J. R. Astron. Soc.* **62**, 195–219.

Otero, J., Wittenberg, R. W., Worthing, R. & Doering, C. R. 2002 Bounds on Rayleigh–Bénard convection with an imposed heat flux. *J. Fluid Mech.* **473**, 191–199.

Perkins, F. W. & Zweibel, E. G. 1987 A high magnetic Reynolds number dynamo. *Phys. Fluids* **30**, 1079–1084.

Rhines, P. B. & Young, W. R. 1983 How fast is a passive scalar mixed within closed streamlines? *J. Fluid Mech.* **133**, 133–145.

Roberts, G. O. 1979 Fast viscous Bénard convection. *J. Geophys. Astrophys. Fluid Dyn.* **12**, 235–272.

Shraiman, B. I. 1987 Diffusive transport in a Rayleigh–Bénard convection cell. *Phys. Rev.* A **36**, 261–267.

Soward, A. M. 1987 Fast dynamo action in a steady flow. *J. Fluid Mech.* **180**, 267–295.

Tejada-Martinez, A. E. & Grosch, C. E. 2007 Langmuir turbulence in shallow water. Part 2. Large-eddy simulation. *J. Fluid Mech.* **576**, 63–108.

Thorpe, S. A. 2004 Langmuir circulation. *Annu. Rev. Fluid Mech.* **36**, 55–79.

Toomre, J., Gough, D. O. & Spiegel, E. A. 1977 Numerical solutions of single-mode convection equations. *J. Fluid Mech.* **79**, 1–31.

Trefethen, L. N. 2000 *Spectral Methods in Matlab*. SIAM.

Waleffe, F. 2001 Exact coherent structures in channel flow. *J. Fluid Mech.* **435**, 93–102.

Wedin, H. & Kerswell, R. 2004 Exact coherent structures in pipe flow: travelling wave solutions. *J. Fluid Mech.* **508**, 333–371.

Wood, W. W. 1957 Boundary layers whose streamlines are closed. *J. Fluid Mech.* **2**, 77–87.